Application of Virtual Noncontrast CT Generation Technology From Intravenous Enhanced CT Based on Deep Learning in Proton Radiotherapy

jianfeng sui
Radiotherapy Department,Second People's Hospital of Changzhou,Nanjing Medical University
Liugang Gao
Radiotherapy Department,Second People's Hospital of Changzhou,Nanjing Medical University
Haijiao Shang
Shanghai Institute of Applied Physics Chinese Academy of Sciences
Chunying Li
Radiotherapy Department,Second People's Hospital of Changzhou,Nanjing Medical University
Zhengda Lu
Radiotherapy Department,Second People's Hospital of Changzhou,Nanjing Medical University
He Mu
Radiotherapy Department,Second People's Hospital of Changzhou,Nanjing Medical University
Tao Lin
Radiotherapy Department,Second People's Hospital of Changzhou,Nanjing Medical University
Kai Xie
Radiotherapy Department,Second People's Hospital of Changzhou,Nanjing Medical University
Jiawei Sun
Radiotherapy Department,Second People's Hospital of Changzhou,Nanjing Medical University
Hui Bi
Radiotherapy Department,Second People's Hospital of Changzhou,Nanjing Medical University
Xinye Ni (nxy2000@aliyun.com)
Radiotherapy Department, Second People's Hospital of Changzhou, Nanjing Medical University, Changzhou 213003; 2 Center for Medical Physics, Nanjing Medical University, Changzhou 213003;

Research

Keywords: deep learning, convolutional neural network, enhanced CT, virtual noncontrast CT, proton radiotherapy

Posted Date: September 8th, 2020

DOI: https://doi.org/10.21203/rs.3.rs-71398/v1

Version of Record: A version of this preprint was published at Journal of Radiation Research and Applied Sciences on March 1st, 2022. See the published version at https://doi.org/10.1016/j.jrras.2022.03.003.

Abstract

Objective: The aim of this study is to generate virtual noncontrast (VNC) computed tomography (CT) from intravenous enhanced CT by using Unet convolutional neural network (CNN). The differences among enhanced, VNC, and noncontrast CT in proton dose calculation were compared.

Methods: A total of 30 groups of CT images of patients who received enhanced and noncontrast CT were selected. Enhanced and noncontrast CT were registered. Among these patients, 20 groups of the CT images were chosen as the training set. Enhanced CT images were used as the input, and the corresponding noncontrast CT images were used as output to train the Unet neural network. The remaining 10 groups of CT images were chosen as the test set. VNC images were generated by the trained Unet neural network. The same proton radiotherapy plan for esophagus cancer was designed based on three images. Proton dose distributions in enhanced, VNC, and noncontrast CT were calculated. The relative dose differences in enhanced CT with VNC and noncontrast CT were analyzed.

Results: The mean absolute error (MAE) of the CT values between enhanced and noncontrast CT was 32.3 ± 2.6 HU. The MAE of the CT values between VNC and noncontrast CT was 6.7 ± 1.3 HU. The mean values of the enhanced CT in the great vessel, heart, lung, liver, and spinal cord were significantly higher than those of noncontrast CT, with the differences of 97, 83, 42, 40, and 10 HU, respectively. The mean values of the VNC CT showed no significant difference with noncontrast CT. The differences among enhanced, VNC, and noncontrast CT in terms of the average relative proton dose for clinical target volume(CTV), heart, great vessels, and lung were also investigated. The average relative proton doses of the contrast CT for these organs were significantly lower than those of noncontrast CT. The largest difference was observed in the great vessel, while the differences in other organs were relatively small. The γ-passing rates of the enhanced and VNC CT were calculated by 2% dose difference and 2 mm distance to agreement. Results showed that the mean γ-passing rate of VNC CT was significantly higher than that of enhanced CT ($p<0.05$).

Conclusions: The proton radiotherapy design based on enhanced CT increased the range error, thereby resulting in calculation errors of the proton dose. Therefore, a technology that can be used to generate VNC CT from enhanced CT based on Unet neural network was proposed. The proton dose calculated based on VNC CT images was essentially consistent with that based on noncontrast CT.

Introduction

Compared with traditional photon therapy, proton beam loses energies when running through materials, and the loss ratio of energy forms a peak at the end of range; this peak is called the Bragg peak. The dose behind the peak drops to zero quickly. Hence, the physical advantages of the proton beam include the fact that the Bragg peak spreading of proton beam is at the lesion of the tumors. Thus, tumors receive the maximum dose of radiation, while normal tissues are exposed to a small radiation dose[1–2]. Given the characteristics of the Bragg peak of proton beam, it has to depict target volume and affects organs

accurately. However, the contrast-enhanced agent should be applied to patients before depiction because the contrast among different soft tissues is generally low. Afterward, enhanced CT images are obtained from CT scanning, which can display tumors or normal organs well. This is of particular importance to esophagus cancer with similar structures close to the target volume.

Traditional proton therapy planning system calculates the proton dose by converting the CT values gained from simulated or planned CT scanning into the stopping power ratio (SPR) of the proton relative to water. Generally, enhanced agent is the thin mixture of high-Z elements (e.g., iodine) and water that may result in the enhanced photoelectric interaction of X-ray during the imaging process, thereby increasing the CT values of the enhanced CT images manually. The enhanced CT images will overestimate practical tissue density and SPR if they are not corrected, thereby causing dose calculation errors.

Generally, the influences of enhanced agent on photon dose distribution can be ignored, and dose can be calculated safely on enhanced CT images[3–5]. Xiao[6] studied the differences between enhanced and noncontrast CT in dose calculation under conformal radiotherapy, intensity modulated radiotherapy, and stereotactic body radiotherapy.This author concluded that enhanced CT achieves the smallest calculation error of the 3DCRT dose and can be applied to calculate the 3DCRT dose directly. However, enhanced agent can influence dose calculation significantly during proton radiotherapy, and another noncontrast CT is needed to formulate the therapy plan[7]. Hwang[8] investigated the influences of enhanced CT on the dose calculation of the proton beam radiotherapy and found that enhanced CT causes as high as 1 cm distal range error of the proton beam. However, the CT values of heart and vessels should be corrected to apply enhanced CT into proton beam radiotherapy, thereby complicating the radiotherapy. Enhanced and noncontrast CT images are not scanned completely at the same time; their registration may also introduce errors. Enhanced and noncontrast CT also increase the dose that is administrated to patients.

Enhanced CT may trigger a large range error if it is applied to calculate the dose of the proton radiotherapy directly. Such range error is often avoided by following two approaches. The first approach makes the rigid registration of enhanced and noncontrast CT images of a patient, then depicts in enhanced CT, and calculates dose on noncontrast CT. However, this approach will generate additional error during registration because enhanced and noncontrast CT are scanned at different times, thereby increasing the uncertainty of proton radiotherapy. The second approach is to generate virtual noncontrast (VNC) images by using dual source CT (DECT) based on the decomposition of the characteristic tissues. Specifically, the decomposition of the characteristic tissues includes the decomposition of the multienergy CT data according to the score of virtual materials (called as characteristic tissues), from which the element composition of human tissues can be estimated[9]. This information can be further used to calculate physical parameters related to dose calculation, such as SPR[10]. The VNC volume of SPR is generated by combining soft tissues and skeleton components, but it neglects the effects of contrast enhanced agent. Such VNC approach requires the attenuation coefficients of contrast enhanced agents of two DECT spectra. It has disadvantages of high complication coefficient, high requirements on

machine performance, and high cost[11]. VNC approach is widely applied in diagnostic imaging[12–14]. Nevertheless, only few studies have discussed the applications of VNC in dose calculation[15, 16].

Recently, deep learning technology based on convolutional neural network (CNN) has been widely applied in medical image processing[17–19]. Many researchers have achieved relatively ideal fruits in image segmentation[20, 21], denoising and artifact removal of the CT images[22], image registration[23, 24], and radiotherapy response prediction[25] by using a deep learning model. For example, in the metal artifact correction of CT, Zhang[26] decreased the metal artifact by introducing it in CNN and achieved satisfying results. In magnetic resonance-guided radiotherapy, Fu[27] generated pseudo-CT images from T1-phase magnetic resonance images based on 2D and 3D CNNs. Gupta[28] generated pseudo-CT images from sagittal MR images by using the Unet neural network and calculated dose distribution based on pseudo-CT and real CT images. The comparison showed that the differences between therapy planned CT and CBCT images and between pseudo-CT and CBCT are − 0.1 and − 0.1 mm, respectively. The differences between left and right axes, between front and rear axes, and between head and tail axes are all − 0.2 mm. However, generating VNC CT by eliminating the enhanced effect from enhanced CT based on deep learning has not been studied to date.

In this study, a method to generate VNC CT images from enhanced CT based on Unet CNN[29] was proposed. Proton dose distributions were also calculated based on noncontrast CT, enhanced CT, and VNC CT images, and the differences were analyzed.

Materials And Methods

A total of 30 groups of CT images of patients who received chest noncontrast and enhanced CT successively were chosen. Siemens CT (Germany) was applied to collect CT images. Scanning parameters are as follows: tube voltage = 110 kVP, tube current = 400 mA, layer thickness = 5 mm, scanning space resolution = 0.72 mm × 0.72 mm to 0.97 mm × 0.97 mm, and size of rebuilt images = 512 × 512. Patients received noncontrast CT first and then enhanced CT immediately. The interval between noncontrast and enhanced CT was shorter than 3 min. To relieve the influences of breathing on images, active breath control, which the act of holding the breath after inhalation, was adopted to all patients during noncontrast and enhanced scanning to decrease differences between noncontrast and enhanced CT images caused by breathing as much as possible.

For each CT image group, noncontrast CT was the fixed image, and enhanced CT was the floating image. The 3D rigid registration of the CT was implemented through 3D affine transformation. Subsequently, registered images were reviewed by a senior radiotherapist to observe the differences in organ and tissue positions between registered noncontrast and enhanced CT. Images with significant differences after registration were eliminated. Finally, 30 groups of CT images of patients were chosen. Each group of images included 60–80 layers of noncontrast CT images and 60–80 layers of registered enhanced CT images.

Unet network was first proposed in the task of biomedical image segmentation and has been widely applied due to a small quantity of training data and good effect. The Unet network structure is shown in Fig. 1. Unet is a symmetrical neural network structure that covers coding and decoding parts. The coding part includes four downsampling processes and can be applied to extract image features. Similarly, the decoding part has four upsampling processes and can restore feature images into the resolution of original images. Unet network applies the 3 × 3 convolutional kernel with a mobile step length of 1. After convolution, the image size was kept constant through the zerofill of the image edges before convolution. Leaky ReLUs was applied as the activation function, and batch normalization was implemented before the activation function. The coding part implemented downsampling by using maximum pooling, and the decoding part implemented upsampling through deconvolution. The input was the enhanced CT images, and the output was the corresponding noncontrast CT images. Among all CT images, 20 groups were chosen as training set, and 10 groups were used as the test set. The training set had 1 200 noncontrast and enhanced CT images, whereas the test set had 600 noncontrast and enhanced CT images. The noncontrast and enhanced CT images were rotated, amplified, and translated in the same way through data enhancement interface of Keras, thereby enhancing the data and increasing the sample size. The sum of the mean absolute (MAE) and square errors was used as the loss function of training, as follows:

where X and Y are the two CT images for comparison, and refers to the CT value of pixel i in the CT image X. A small batch gradient descent optimization algorithm was applied in the training, in which the batch size was set 12.

In this study, the proton dose was calculated by the Monte Carlo algorithm at the computational grid of 2 mm. During dose calculation, the planning system software (RayStation) can achieve SPR automatically according to the composition of different materials. Different materials were obtained according to the CT-HU scale curve. The scale curve is shown in Fig. 2.

Ten patients in the test set were subjects with esophagus cancer that require radical radiotherapy. The noncontrast CT images and enhanced images of 10 groups of patients and VNC CT images generated by Unet neural network were inputted into RayStation. Senior doctors were invited to depict target radiotherapy volume and important protection organs (e.g., heart, great vessel, lung, liver, and spinal cord) on noncontrast CT images. Afterward, the depicted target radiotherapy volume and protection organs were copied to enhanced and VNC CT images to compare the mean CT of different organs on enhanced, VNC, and noncontrast CT images.

Patients were exposed to radiation on a proton accelerator. Clinical target volume(CTV) was provided with the prescription doses of 6 000 cGy, and the number of treatments was set to 30. The maximum dose in the target volume was lower than 105%. During the design of the proton therapy plan, two to three fields were chosen according to the position of the tumors. For example, the three radiation fields of 0°, 220°, and 130° can be chosen for angle distribution when the tumor was at the mediastinum. The therapy plan design is shown in Fig. 3. First, the radiotherapy plan was designed and optimized on noncontrast CT images, and the dose distribution was calculated. Second, the radiotherapy plan was copied into the

enhanced and VNC CT images. Under this circumstance, dose distribution was calculated directly without plan optimization. Finally, proton dose distributions on enhanced, VNC, and noncontrast CT images were compared. Mean CT and dose were calculated using the Wilcoxon matched pair rank test.

Results

The training of the Unet neural network stops after 2 000 trainings into data in the entire training set, thereby reaching 200 000 iterations. Enhanced CT images in the test set are inputted into the trained Unet neural network to generate VNC CT images. Enhanced, VNC, and noncontrast CT images on the same layer are shown in Fig.4. The window level and width of CT are 40 and 400 HU, respectively. Enhanced CT images are brighter than noncontrast CT images at the great vessel, while VNC CT images are extremely similar to noncontrast CT images.

Deducting noncontrast CT from enhanced CT images showed that the CT values of several organs in enhanced CT images are significantly higher than those in noncontrast CT images. This result is attributed to the absorption of the contrast agent. The difference between noncontrast and VNC CT through deduction is small. A statistical analysis on the MAEs (HU) of the enhanced CT with those of VNC and practical noncontrast CT of 10 patients in the test set is carried out. When the air region other hand human body is excluded, the MAE between contrast and noncontrast CT is 32.3 ± 2.6 HU, while the MAE between VNC and practical noncontrast CT is 6.7 ± 1.3 HU. This result shows that the contrast agent can intensify the difference between enhanced and noncontrast CT. However, the VNC CT that is generated from enhanced CT based on Unet neural network shows a small difference with practical noncontrast CT.

The inconsistent range curves of enhanced, VNC, and noncontrast CT when the 150° radiation field runs through the heart are shown in Fig. 5. The figure shows that the range error between noncontrast and VNC CT is relatively small, while those of the enhanced CT with noncontrast and VNC CT are relatively large. During radiotherapy design, the uncertainty of proton positioning error at the upper and lower, left and right, and head and tail is 5 mm. The range uncertainty is ± 3.5%.

Statistics on the mean CT values of enhanced, VNC, and noncontrast CT images in the heart, great vessel, lung, liver, and spinal cord are shown in Table 1. In enhanced CT images, the CT values of the heart, great vessel, lung, liver, and spinal cord are significantly higher than those observed in noncontrast CT images ($p < 0.05$). The largest difference (97 HU) is observed in the great vessel, followed by the heart (83 HU). The differences in the lung, liver, and spinal cord are 42, 40, and 10 HU, respectively. However, the differences in HU value between VNC and practical noncontrast CT are not significant. The difference in the lung is 4 HU, while those in the heart, great vessel, liver, and spinal cord are smaller than 2 HU.

Table 1
Mean CT values of three types of images in different organs

	mean CT values of heart, great vessel, lung, liver and spinal cord(HU)				
	heart	great vessel	lung	liver	spinal cord
noncontrast CT	26.5 ± 5.2	42.6 ± 2.3	-698.6 ± 65.8	52.4 ± 4.6	31.2 ± 2.3
Enhanced CT	109.2 ± 16.2	139.3 ± 14.8	-656.4 ± 76.3	92.2 ± 8.7	41.1 ± 3.7
VNC CT	25.2 ± 6.8	41.3 ± 3.9	-702.4 ± 72.7	52.8 ± 6.5	32.6 ± 2.7

The calculated dose distribution in enhanced, VNC, and noncontrast CT images in the CTV, heart, great vessel, and lung is shown in Table 2. The dose of the noncontrast CT is used as the standard. The dose of the enhanced CT in different tissues is subtracted to the dose of noncontrast CT in the corresponding tissues and then averaged; the result is then referred to as the Former. Similarly, the dose of VNC CT in different tissues is subtracted to the dose of the noncontrast CT in corresponding tissues and then averaged; the result was then referred to as the Later. As listed in Table 2, the mean of the Former is higher than that of the Later, and the Former is a negative value. This result indicated that the dose of enhanced CT at these positions is significantly lower than that of noncontrast CT. The largest difference in the relative mean dose is observed in the great vessel, while the difference in other organs is relatively small. The difference in mean dose between VNC and noncontrast CT is relatively small. Hence, this difference can be ignored.

Table 2
Differences in the mean relative dose among enhanced, VNC, and noncontrast CT

	Differences of relative dose mean with noncontrast CT(cGy)			
	relative dose mean of CTV	relative dose mean of heart	relative dose mean of great vessel	relative dose mean of lung
Enhanced CT-noncontrast CT	-7.6 ± 35.9	-57.6 ± 70	-150.8 ± 140.9	-29.6 ± 30.4
VNC CT-noncontrast CT	0.1 ± 5.8	-15.4 ± 25.3	1.4 ± 10	-5.6 ± 9.1

The sectional dose distributions of a typical patient based on enhanced, VNC, and noncontrast CT images are shown in Fig. 6. The dose distributions based on VNC and noncontrast CT are essentially similar. However, the dose distribution based on enhanced CT has significant differences compared with those based on noncontrast and VNC CT. The dose line of 6 000 cGY in noncontrast and VNC CT has a relatively high target fitness, whereas the target fitness of enhanced CT is relatively poor.

The dose–volume histograms (DVH) of different organs based on enhanced, VNC, and noncontrast CT are shown in Fig. 7. The DVH based on VNC and practical noncontrast CT is essentially similar, while that

based on enhanced CT differed significantly from those based on VNC and practical noncontrast CT. Such difference is mainly evident in the CTV and great vessel.

The comparison of γ-passing rates between enhanced and VNC CT is shown in Fig. 8. The dose distribution based on noncontrast CT is used as the standard value. The dose difference is 2%, and the distance to agreement is 2 mm. The γ-passing rates of enhanced and VNC CT are shown in Fig. 8. The mean γ-passing rate of the VNC CT is significantly higher than that of enhanced CT (0.981 vs 0.934, $p < 0.05$). The γ distribution pattern in the enhanced CT image surrounding the high-dose region is significantly different from that in the noncontrast CT image, but it is less different from that in VNC CT.

Discussions

Contrast agent might influence the accuracy of dose calculation during proton radiotherapy planning based on enhanced CT. The aim of this study is to investigate the influences of VNC CT on the dose calculation of proton radiotherapy in increasing the dose calculation accuracy by the virtual elimination of contrast agent in enhanced CT. Experimental results verify the feasibility of the proposed method. The difference in dose based on VNC and noncontrast CT is small. Such difference is significantly smaller than the difference in dose based on enhanced and noncontrast CT. Hence, proton radiotherapy plan can be constructed directly based on VNC CT. As a promising technology, VNC CT based on deep learning can transform enhanced CT into VNC CT through the Unet neural network, thereby decreasing the radiation dose to patients. VNC CT possesses promising application prospects in clinics.

In this study, 20 groups of CT images of patients were used to train the network when generating VNC CT from enhanced CT. Relatively few datasets and training effect can be improved by increasing the training set. Training accuracy could be improved by several improved networks based on Unet [30–32] or confront neural network GAN[33]. This MAE could also be caused by partial deformation difference after the registration of enhanced and noncontrast CT. Although this study has adopted a series of measures, including controlling the interval between enhanced and noncontrast CT (< 3 min), requiring patients to hold breath during scanning, and eliminating images with significant differences after registration by senior doctors, the difference in deformation caused by the movement of organs is inevitable. On the one hand, the difference in deformation leads to poor accuracy of the training network. On the other hand, the difference in deformation is transferred from enhanced CT into VNC CT during the test, and the incomplete superposing between VNC and noncontrast CT in several edges may increase MAE. To increase the applicability of VNC CT to clinics, an advanced scheme should be developed and verified. This deformation difference can be solved by an adaptive method in the future.

Conclusions

This study proposes a new strategy to increase the accuracy of proton radiotherapy plan on the based on VNC CT. The profiles of target volume and affected organs can be distinguished well by using a contrast agent. However, proton radiotherapy plan design based on enhanced CT can decrease the calculation

accuracy of the dose. The VNC CT, which is generated from enhanced CT based on Unet convolutional neural network, is extremely similar to practical noncontrast CT. Proton dose distribution can be calculated accurately based on VNC CT images.

Abbreviations

VNC:virtual noncontrast;CT:computed tomography;CNN:convolutional neural network;MAE:mean absolute error;CTV:clinical target volume;SPR:stopping power ratio;DECT:dual source computed tomography;CBCT:cone beam computed tomography;DVH:dose–volume histograms

Declarations

Acknowledgments

We acknowledge all the investigators, patients and their families.

Authors' contributions

Ni Xinye: conceived and designed the study, edited and reviewed the manuscript. All authors read and approved the final manuscript;Sui Jianfeng and Gao Liugang contributed equally to this work, participated in the design of the study, carried out the study, performed the statistical analysis, and drafted the manuscript;Shang Haijiao, Li Chunying, Lu Zhengda , He Mu,Lin Tao, Xie Kai , Sun Jiawei and Bi Hui: helped to carried out the study.

Funding

This work was supported by the High-Level Medical Talents Training Project of Changzhou (grant no: 2016CZLJ004) , Changzhou Key Laboratory of Medical Physics, China (grant no. CM20193005) ,Youth Project of Changzhou Municipal Commission of Health and Family Planning (grant no: QN201718) and Funding from Young Talent Development Plan of Changzhou Health Commission(CZQM2020075)

Availability of data and materials

The data and materials of this study are available from the corresponding author on reasonable request.

Ethics approval and consent to participate

This study was approved by the Research Ethics Board of the Second People's Hospital of Changzhou, Nanjing Medical University. Written informed consent to participate in this study was not required in accordance with national and institutional guidelines.

Consent for publication

Not applicable.

Competing interests

None declared.

Author details

[1] Radiotherapy Department, Second People's Hospital of Changzhou, Nanjing Medical University, Changzhou 213003;

[2] Center for Medical Physics, Nanjing Medical University, Changzhou 213003; [3] Shanghai Institute of Applied Physics, Chinese Academy of Sciences,Shanghai 201800; [4] School of biomedical engineering and informatics, Nanjing Medical University, Nanjing 213000;

References

1. Muzik J, Soukup M. Markus Alber. Comparison of fixed-beam IMRT, helical tomotherapy, and IMPT for selected cases.Med Phys,2008,35(4):1580–92.doi: 10.1118/1.2890085.
2. Zhang X, Li Y, Pan X, et al. Intensity-modulated proton therapy reduces the dose to normal tissue compared with intensity-modulated radiation therapy or passive scattering proton therapy and enables individualized radical radiotherapy for extensive stage IIIB non-small-cell lung cancer: a virtual clinical study. Int J Radiat Oncol Biol Phys. 2010;77(2):357–66. doi:10.1016/j.ijrobp.2009.04.028.
3. U Ramm 1. Damrau M, Mose S,et al. Influence of CT contrast agents on dose calculations in a 3D treatment planning system. Phys Med Biol. 2001, 46(10):2631–5.doi:10.1088/0031-9155/46/10/308.
4. Choi Y, Kim J-K, Lee H-S, et al. Influence of intravenous contrast agent on dose calculations of intensity modulated radiation therapy plans for head and neck cancer. Radiother Oncol. 2006;81(2):158–62. doi:10.1016/j.radonc.2006.09.010.
5. Yuta Shibamoto A, Naruse H, Fukuma, et al. Influence of contrast materials on dose calculation in radiotherapy planning using computed tomography for tumors at various anatomical regions: A prospective study. Radiother Oncol. 2007;84(1):52 – 5. doi:10.1016/j.radonc.2007.05.015.
6. Jianghong Xiao H, Zhang Y, Gong, et al, Feasibility of using intravenous contrast-enhanced computed tomography (CT) scans in lung cancer treatment planning.Radiother Oncol, 2010, 96(1):73 – 7.doi: 10.1016/j.radonc.2010.02.029.
7. Hansjörg Wertz O, Jäkel. Influence of iodine contrast agent on the range of ion beams for radiotherapy. Med Phys. 2004;31(4):767–73. doi:10.1118/1.1650871.
8. Hwang U-J, Shin DH, Kim TH, et al. The effect of a contrast agent on proton beam range in radiotherapy planning using computed tomography for patients with locoregionally advanced lung cancer. Int J Radiat Oncol Bio Phys. 2011;81(4):e317-24. doi:10.1016/j.ijrobp.2011.02.025.

9. Lalonde A, Bouchard H. A general method to derive tissue parameters for Monte Carlo dose calculation with multi-energy CT. Phys Med Bio. 2016;61(22):8044–69. doi:10.1088/0031-9155/61/22/8044.
10. Arthur Lalonde E, Bär H, Bouchard. A Bayesian approach to solve proton stopping powers from noisy multi-energy CT data. Med Phys. 2017;44(10):5293–302. doi:10.1002/mp.12489.
11. Arthur Lalonde Y, Xie B, Burgdorf, et al. Influence of intravenous contrast agent on dose calculation in proton therapy using dual energy CT. Phys Med Bio. 2019;64(12):125024. doi:10.1088/1361-6560/ab1e9d.
12. Zhang L-J, Peng J, Wu S-Y, et al. Liver virtual non-enhanced CT with dual-source, dual-energy CT: A preliminary study. Eur Radiol. 2010;20(9):2257–64. doi:10.1007/s00330-010-1778-7.
13. Toepker M, Moritz T, Krauss B, et al. Virtual non-contrast in second-generation, dual-energy computed tomography: Reliability of attenuation values. Eur J Radiol. 2012;81(3):e398–405. doi:10.1016/j.ejrad.2011.12.011.
14. Sebastian Faby SK. Stefan Sawall ,et al.Performance of today's dual energy CT and future multi energy CT in virtual non-contrast imaging and in iodine quantification: A simulation study. Med Phys. 2015;42(7):4349–66. doi:10.1118/1.4922654.
15. Sachiko Yamada T, Ueguchi T, Ogata, et al. Radiotherapy treatment planning with contrast-enhanced computed tomography: feasibility of dual-energy virtual unenhanced imaging for improved dose calculations. Radiat Oncol,2014, 9:168.doi: 10.1186/1748-717X-9-168.
16. Andréanne L. ,Arthur Lalonde,Houda Bahig,et al. Robust quantitative contrast-enhanced dual-energy CT for radiotherapy applications.Med Phys, 2018, 45(7): 3086–3096.doi: 10.1002/mp.12934.
17. Berkman Sahiner A, Pezeshk, Lubomir M, Hadjiiski, et al. Deep learning in medical imaging and radiation therapy. Med Phys. 2019;46(1):e1–36. doi:10.1002/mp.13264.
18. Matteo Maspero, Mark HF, Savenije, Anna M, Dinkla, et al. Dose evaluation of fast synthetic-CT generation using a generative adversarial network for general pelvis MR-only radiotherapy. Phys Med Biol. 2018;63(18):185001. doi:10.1088/1361-6560/aada6d.
19. Xiao Han. MR-based synthetic CT generation using a deep convolutional neural network method. Med Phys. 2017;44(4):1408–19. doi:10.1002/mp.12155.
20. Kovacs W, Roth NHsieh,H ,et al. Holistic segmentation of the lung in cine MRI.J Med Imaging (Bellingham).20174(4):041310. doi: 10.1117/1.JMI.4.4.041310.
21. Amal Farag, Le Lu, Holger R, Roth, et al. A Bottom-Up Approach for Pancreas Segmentation Using Cascaded Superpixels and (Deep) Image Patch Labeling. IEEE Trans Image Process. 2017;26(1):386–99. doi:10.1109/TIP.2016.2624198.
22. Kyong Hwan Jin MT, McCann E, Froustey,et al. Unser, Deep Convolutional Neural Network for Inverse Problems in Imaging. IEEE Trans Image Process. 2017;26(9):4509–22. doi:10.1109/TIP.2017.2713099.
23. Guorong Wu M, Kim Q, Wang, et al.Unsupervised deep feature learning for deformable registration of MR brain images.Med Image Comput Assist Interv,2013,16(Pt 2): 649 – 56.doi: 10.1007/978-3-642-

40763-5_80.

24. Lv J, Yang M, Zhang J ,et al. Respiratory motion correction for free-breathing 3D abdominal MRI using CNN-based image registration: a feasibility study. Br J Radio. 2018;91(1083):20170788. doi:10.1259/bjr.20170788.
25. Nielsen A, Tietze MBoH,A,et al. Prediction of Tissue Outcome and Assessment of Treatment Effect in Acute Ischemic Stroke Using Deep Learning,Stroke,201849(6): 1394–1401.doi: 10.1161/STROKEAHA.117.019740.
26. Zhang Y, Yu H. Convolutional Neural Network based Metal Artifact Reduction in X-ray Computed Tomography. IEEE Trans Med Imaging. 2018;37(6):1370–81. doi:10.1109/TMI.2018.2823083.
27. Fu J, Yang Y, Singhrao K, et al. Deep learning approaches using 2D and 3D convolutional neural networks for generating male pelvic synthetic computed tomography from magnetic resonance imaging. Med Phys. 2019;46(9):3788–98. doi:10.1002/mp.13672.
28. Dinank Gupta M, Kim, Karen A, Vineberg, et al. Generation of Synthetic CT Images From MRI for Treatment Planning and Patient Positioning Using a 3-Channel U-Net Trained on Sagittal Images. Front Oncol. 2019;9:964.doi. 10.3389/fonc.2019.00964.
29. Ronneberger O, Fischer P, Brox T, et al. U-Net: Convolutional Networks for Biomedical Image Segmentation. medical image computing and computer assisted intervention, 2015: 234–241.doi: 10.1007/978-3-319-24574-4$428.
30. 10.1007/978-3-030-00889-5_1
    Zongwei Zhou MdMRahmanS, Tajbakhsh N, et al, UNet++: A Nested U-Net Architecture for Medical Image Segmentation. Deep Learn Med Image Anal Multimodal Learn Clin Decis Support (2018), 2018,11045:3–11.doi: 10.1007/978-3-030-00889-5_1.
31. Li X, Chen H, Qi X, et al. H-Dense UNet: Hybrid Densely Connected UNet for Liver and Tumor Segmentation from CT Volumes. IEEE Trans Med Imaging. 2018;37(12):2663–74. doi:10.1109/TMI.2018.2845918.
32. Oktay O, Schlemper J, Folgoc LL, et al. Attention U-Net: Learning Where to Look for the Pancreas. arXiv: Computer Vision and Pattern Recognition, 2018,1–8.arXiv:1804.03999.
33. Arjovsky M, Chintala S, Bottou L. Wasserstein Generative Adversarial Networks, international conference on machine learning,2017, 214–223.

Figures

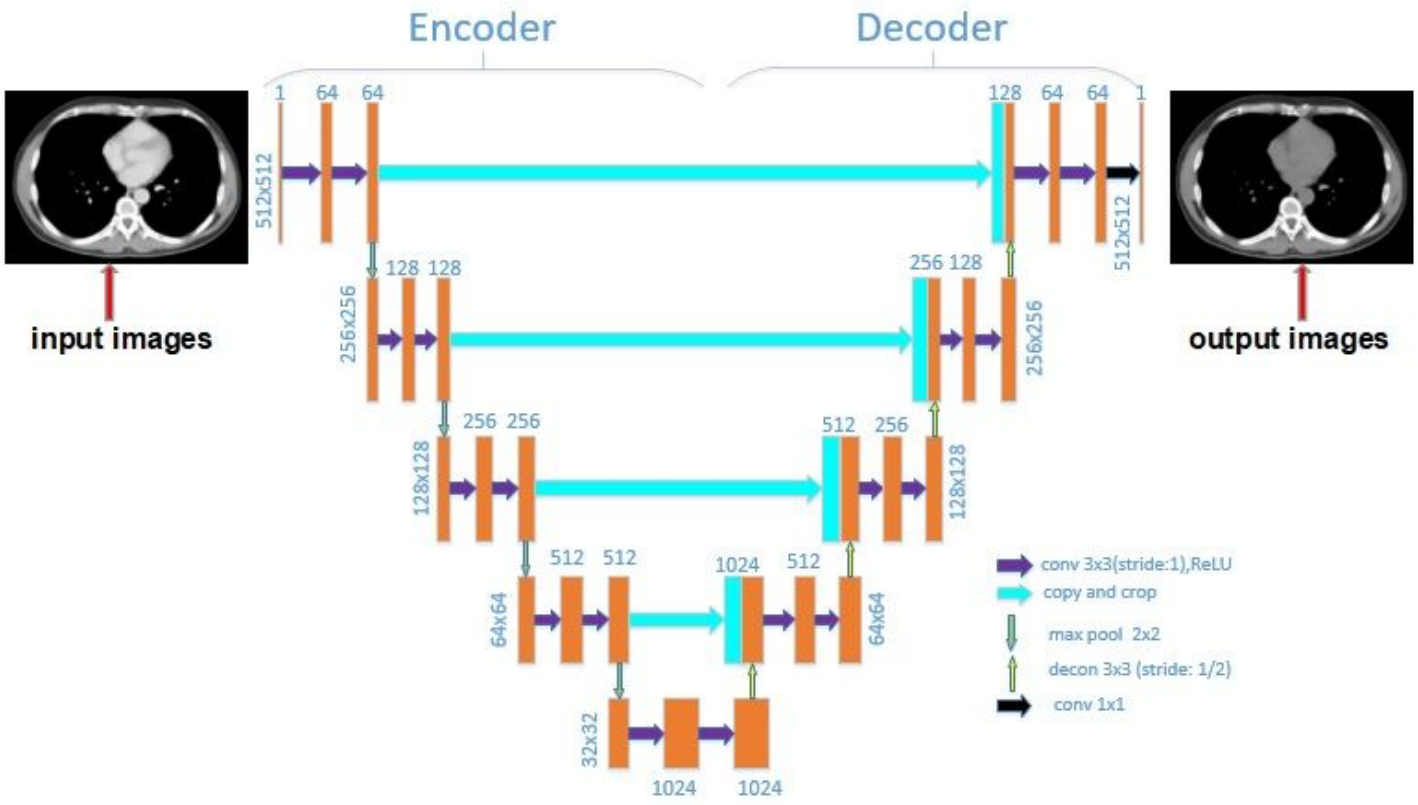

Figure 1

Structure of Unet convolutional neural network

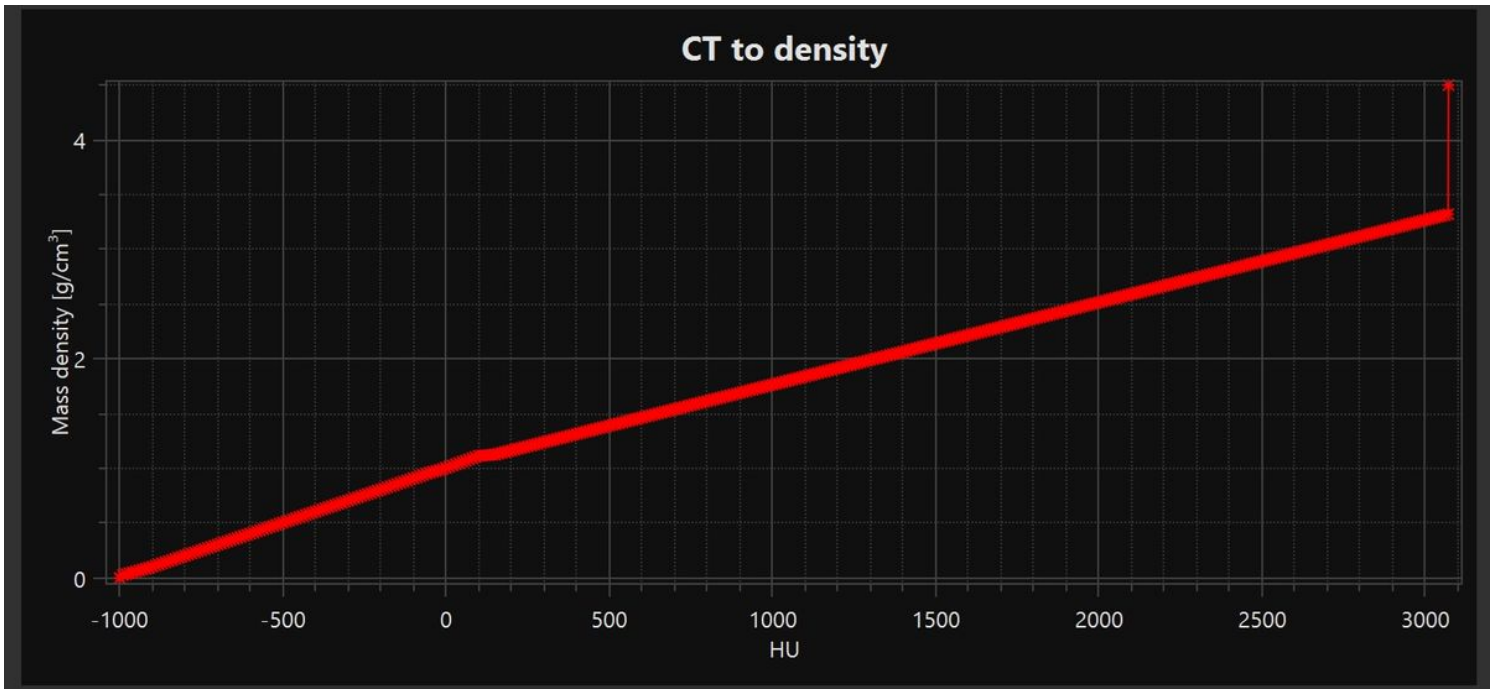

Figure 2

Scale curve of CT-HU

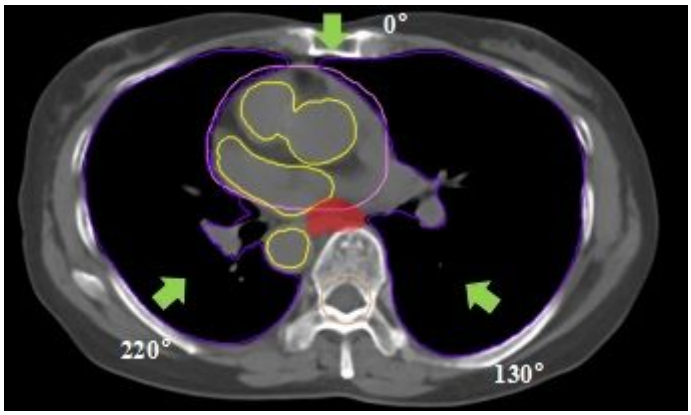

Figure 3

Design of proton radiotherapy plan

Figure 4

Comparison of three types of CT images on same layer a: Practical noncontrast CT images, b: enhanced CT images, and c: VNC CT images generated through Unet neural network

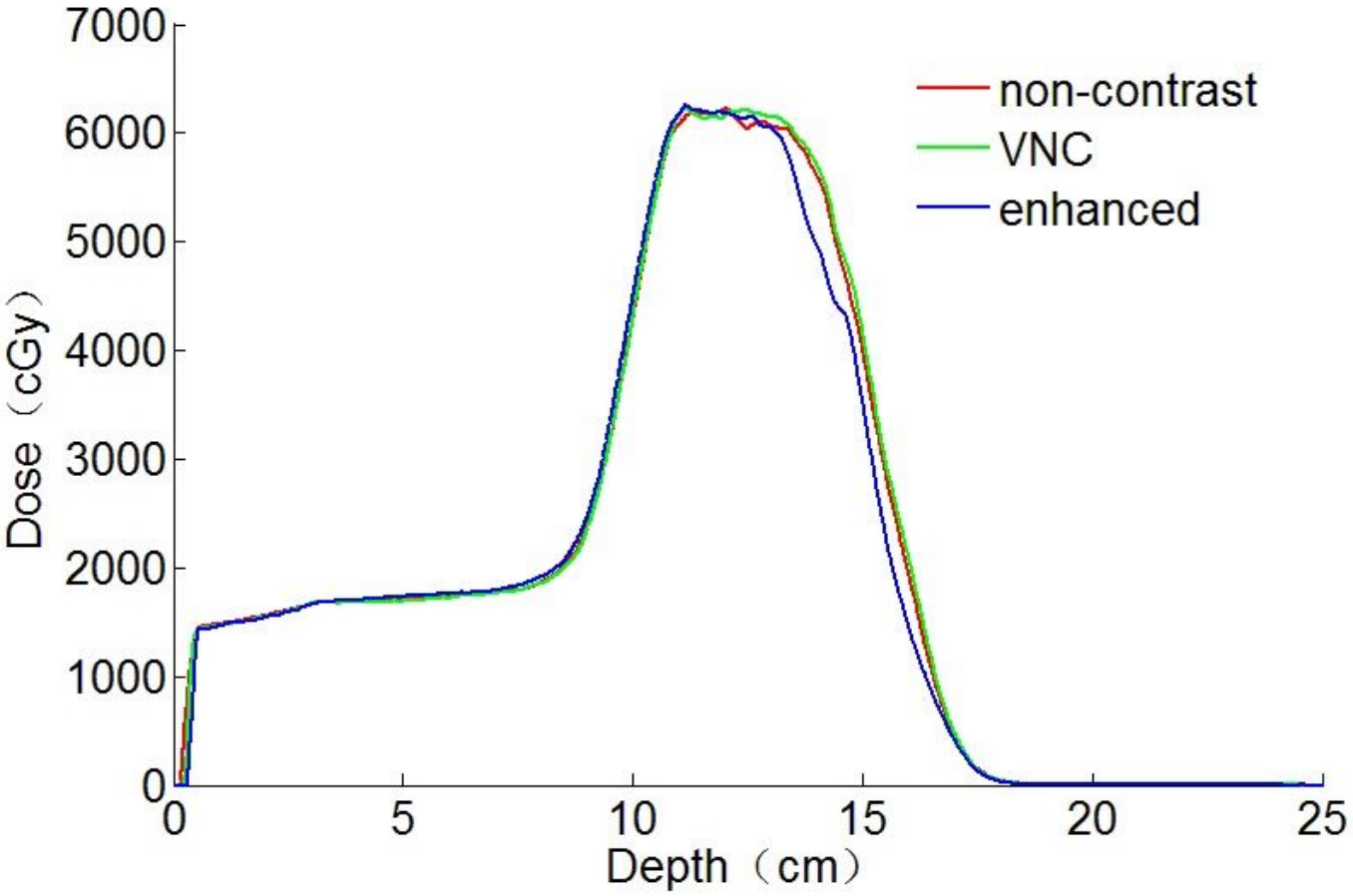

Figure 5

Variations of ranges of enhanced, VNC, and noncontrast CT

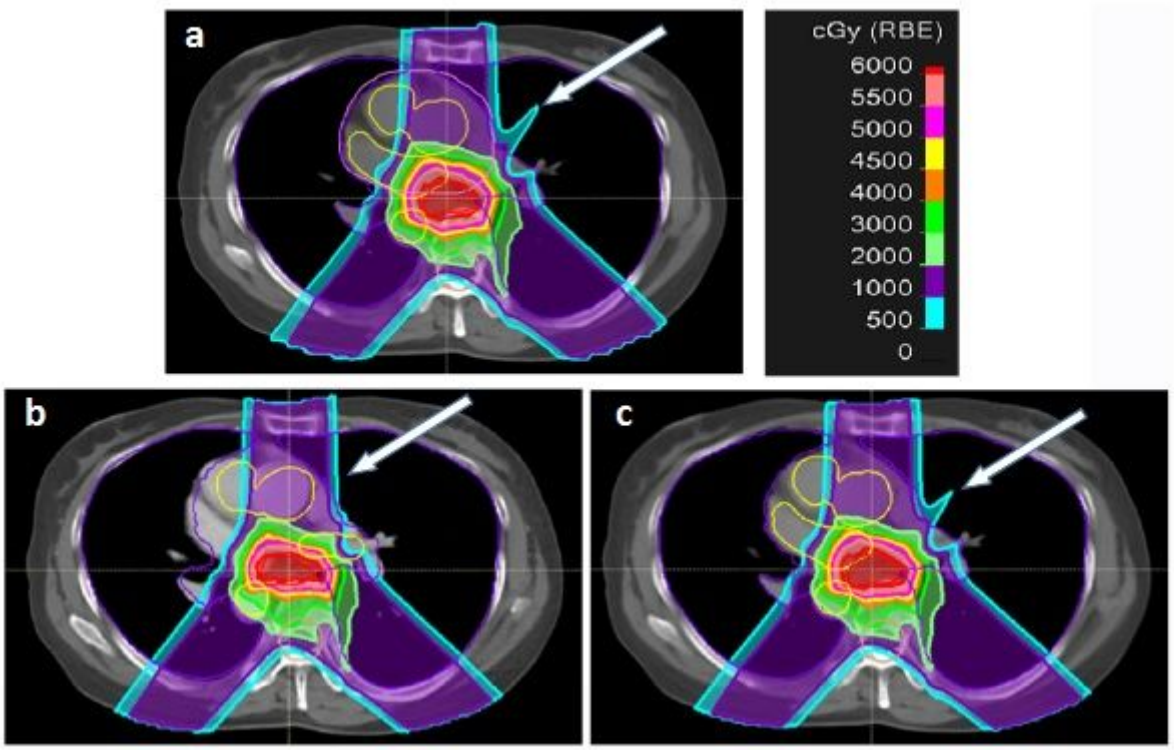

Figure 6

Sectional dose distribution based on enhanced, VNC, and noncontrast CT. a: Dose based on noncontrast CT, b: dose based on enhanced CT, and c: dose based on VNC CT

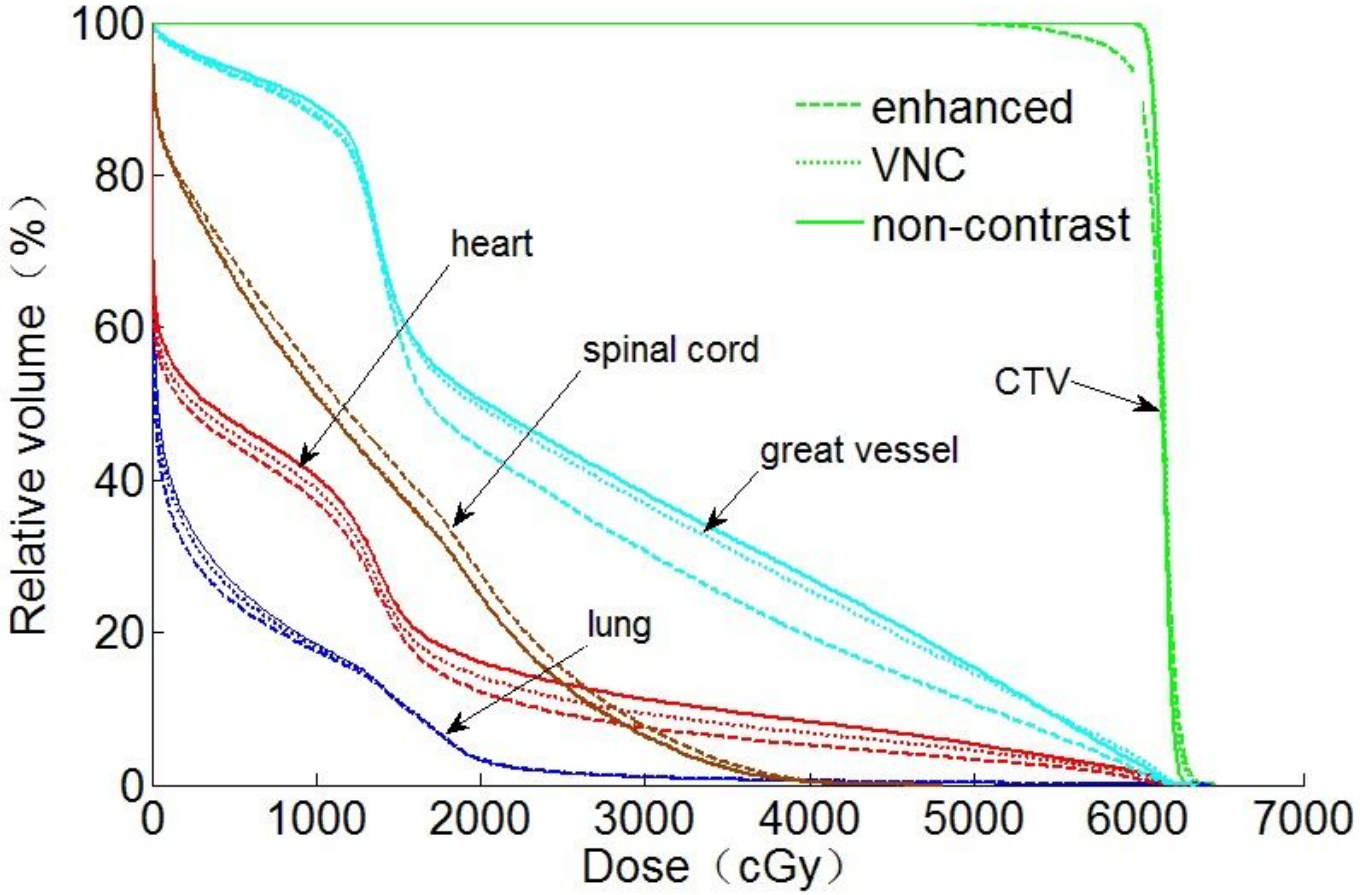

Figure 7

DVH of different organs based on enhanced, VNC, and noncontrast CT

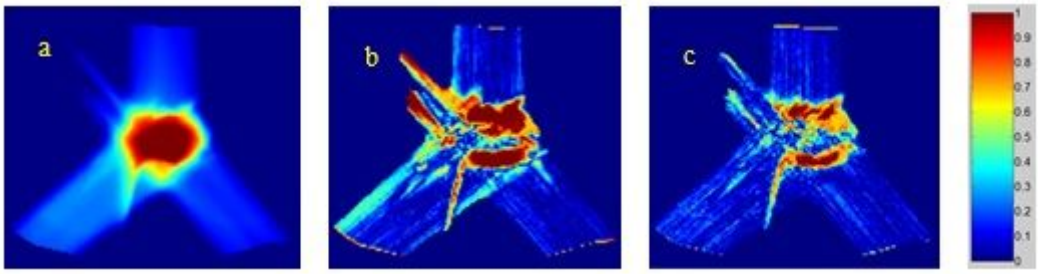

Figure 8

Distributions of γ-passing rates of enhanced and VNC CT